in diameter are clearly seen. The hole density is 7×10^8 cm^{-2}. The surface of this film is considerably rougher than that of polycarbonate or polyethylene terephthalate. There are protuberances like mountain chains. The roughness is a characteristic of the original film and remains unaltered after irradiation and chemical etching. We do not believe that the roughness has any effect on the etching of fission tracks. Figure 1b is an electron micrograph of another film irradiated in vacuum and etched under the same conditions as in Fig. 1a. In this case there is almost no indication of chemical etching. A detailed examination, however, shows the existence of obscure dark spots, which are etched tracks in their earlier stage of enlargement.

A comparison of Fig. 1, a and b, indicates the effectiveness of oxygen for enhancing the preferential etching rate. The reaction of oxygen with active species formed by the passage of fission fragments must be occurring during bombardment of fission fragments as well as during the cooling time after irradiation.

The hole density can be calculated from the irradiating condition by the use of the formula

$$\rho = 2N\sigma\phi tA/S$$

where ρ is the hole density, N is the number of ^{235}U atoms, σ is the fission cross section of ^{235}U for thermal neutron, ϕ is the thermal neutron flux, t is the irradiation time, A is the fraction of fission fragments that enters into the film, and S is the irradiation area. The value of A, determined by the geometry of the collimator, is 1/70 in the present experiments. The calculation gives $\rho = 3.0 \times 10^8$ cm^{-2}, which is comparable with the observed density in Fig. 1a.

We also took transmission electron micrographs with a high-voltage electron microscope (Japan Electron Optics Laboratory Co. Ltd., 1000 kv) in order to see the growth of etched tracks across the film. A specimen 9 μm thick was directly observed. Several circular spots glittered intensely, and many somewhat opaque patterns of various lengths were recognized. When the specimen was tilted several degrees, the spots changed to opaque patterns whose lengths increased with the angle of inclination. At the same time some of the opaque patterns became shorter in length and changed to spots. We believe that the spots that glitter are due to the passage of the electron beam through the holes, which are oriented exactly parallel to the beam direction. The opaque patterns are the images of the holes inclined to the electron beam. We also determined that the etched tracks penetrated the film by detecting the passage of gases and aqueous solutions through the film.

The chemical etching of the charged particle tracks has been studied in various dielectric materials, and etching methods are now widely used in the detection of charged particles as well as in many technological applications (*2*). Monnin (*3*) has examined the chemical etching in polyethylene, polyvinyl chloride, polyvinyl-polyvinylidene chloride copolymer, and several other plastics, but polyfluoro plastics were not included. Bopp (*4*) attempted the chemical etching of α-particle tracks in polytetrafluoroethylene, polychlorotrifluoroethylene, and polyvinylidene fluoride under severe etching conditions (concentrated sulfuric acid at 300°C and 50 percent sodium hydroxide solution at 155°C) but could not find etch pits in any of the polyfluoro plastics. Maybury and Libby (*5*) revealed fission tracks in polytetrafluoroethylene by graft copolymerization of acrylic acid and by the fixation of dye so that its fluorescence could be observed under ultraviolet light. Chemical etching was not used.

The rate at which the track width in polyvinylidene fluoride enlarges, obtained by dividing the hole diameter by the etching time in Fig. 1a, is 1.7 nm/hour. The value is smaller by almost three orders of magnitude than the corresponding rate in polycarbonate or polyethylene terephthalate. It seems unlikely that polyvinylidene fluoride will develop holes several micrometers in diameter by practical experimental procedures, sufficient to permit them to be seen under an optical microscope. A slow etching rate is anticipated for all polyfluoro plastics. Probably polyfluoro plastics are suitable for the formation of a membrane filter with fine holes a few hundred nanometers or less in diameter.

YOSHIHIDE KOMAKI
SHIGEO TSUJIMURA
Division of Chemistry, Japan Atomic Energy Research Institute, Tokai-mura, Naka-gun, Ibaraki-ken, Japan

References and Notes

1. K. Makuuchi, T. Seguchi, T. Suwa, T. Abe, N. Tamura, M. Takehisa, *Nippon Kagaku Kaishi* **1973**, 1574 (1973); T. Seguchi, K. Makuuchi, T. Suwa, N. Tamura, T. Abe, M. Takehisa, *ibid.* **1974**, 1309 (1974).
2. R. L. Fleischer, P. B. Price, R. M. Walker, *Nuclear Tracks in Solids, Principle and Applications* (Univ. of California Press, Berkeley, 1975).
3. M. Monnin, thesis, Université de Clermont-Ferrand (1969); ——— and D. B. Isabelle, *Ann. Phys. Biol. Med.* **4**, 95 (1970).
4. C. D. Bopp, *Oak Ridge Natl. Lab. Rep. 4351* (1969), p. 25.
5. P. C. Maybury and W. F. Libby, *Nature (London)* **254**, 209 (1975).
6. We thank K. Ogura and H. Otsuji of Japan Electron Optics Laboratory Co. Ltd. for taking micrographs with the field emission scanning electron microscope and H. Ohtsu of the Japan Atomic Energy Research Institute for his help in the high-voltage electron microscopy.

21 April 1977; revised 7 September 1977

A Fluorite Isotype of SnO_2 and a New Modification of TiO_2: Implications for the Earth's Lower Mantle

Abstract. *The existence of a cubic fluorite-type SnO_2 and a hexagonal TiO_2 (which may be related to the fluorite structure) have been demonstrated by an in situ x-ray diffraction study in which a diamond-anvil pressure cell was used after the samples had been heated by a continuous yttrium-aluminum-garnet laser. At room temperature, the lattice parameter for SnO_2 (fluorite) is* a = *4.925 ± 0.005 angstroms and those for TiO_2 (fluorite-related) are* a = *9.22 ± 0.01 angstroms and* c = *5.685 ± 0.006 angstroms at about 250 kilobars. The volume change associated with the transition from rutile to fluorite (or related structure) is about −8 percent for SnO_2 and −10.5 percent for TiO_2 at transition. Upon release of pressure, both the fluorite-type SnO_2 and the TiO_2 reverted to the α-PbO_2 structure at room temperature. The hypothesis that the earth's lower mantle is composed of oxide phases might be feasible if it were possible for SiO_2 to possess the fluorite structure or its related forms at high pressure, as shown for SnO_2 and TiO_2 in this study. The oxide hypothesis proposed here differs from that postulated by Birch in that the primary coordination of silicon is 6 for Birch's hypothesis and 8 for the hypothesis presented here.*

Because of the stoichiometric similarity between SiO_2 and TiO_2, Thompson predicted in 1952 that SiO_2 might crystallize in the rutile (TiO_2) structure at high pressure; this idea was partly the basis of Birch's hypothesis that the earth's lower mantle consisted predominantly of oxide phases (*1*). Stishov and Popova (*2*) later synthesized the rutile form of SiO_2, which was subsequently named stishovite (*3*). Further phase transformation of stishovite to the fluorite structure has

0036-8075/78/0127-0422$00.50/0

been suggested (*4*). A recent recovery shock-wave experiment at pressures from 700 to 900 kbar, however, indicated the occurrence of a α-PbO_2 structure of SiO_2 (*5*). In contrast to this, Liu *et al.* have found the modified niccolite form of SiO_2 in a static high-pressure experiment (*6*).

Despite the existing ambiguities in the formation of the α-PbO_2 form of SiO_2 (*6*), the α-PbO_2 structure has been ubiquitously found as the postrutile phase in the dioxides PbO_2 (*7*), SnO_2 (*8*), and TiO_2 (*9*) and in the difluorides MnF_2 (*10*) and ZnF_2 (*11*) in static high-pressure quench experiments. In situ x-ray analysis of the difluorides, however, has revealed that the α-PbO_2 forms occurred only upon the release of pressure, and the true high-pressure phase was considered to be a distorted fluorite structure (*12*).

If one accepts the use of difluorides as analogs to SiO_2 with respect to phase behavior, it follows that phase transformations found in dioxides provide better candidates for SiO_2. In light of the finding from in situ x-ray diffraction studies of the difluorides, the true postrutile phase of PbO_2 (*7*), SnO_2 (*8*), and TiO_2 (*9*), if one exists, should be investigated.

Of these dioxides, the stability field for the α-PbO_2 form of PbO_2 might be real since the fluorite isotype of PbO_2 has also been synthesized at still higher pressures (*4*). The transition from rutile to α-PbO_2 found in SnO_2 and TiO_2 is somewhat doubtful, since shock-wave studies on SnO_2 (*13*) and TiO_2 (*14*) indicate a large volume change. Hugoniot data for both SnO_2 and TiO_2 indicate a phase transition accompanied by a decrease of some 30 percent in the zero-pressure volume, whereas the volume change associated with the transition from rutile to α-PbO_2 is only about 1 to 2 percent. On the basis of these observations, I have earlier concluded that the quenched α-PbO_2 forms of SnO_2 and TiO_2 are not the large transition, or transitions, revealed by shock-wave experiments (*8*).

In the present work, I have investigated the postrutile phases of both SnO_2 and TiO_2 by in situ x-ray analysis, using a diamond-anvil pressure cell. The starting samples of SnO_2 and TiO_2 were identical to those used in my earlier work (*8*). The procedure of sample preparation was also the same. Finely powdered samples were compressed in a UP-type diamond-anvil cell (*15*) and heated by a continuous yttrium-aluminum-garnet laser. The loading pressures of the sample at the central portion of the anvil were estimated on the basis of the position of the driving piston, which had been earlier calibrated with NaCl used as the internal pressure standard. Loading pressures thus estimated are probably accurate to only ± 15 percent. Sample temperatures were estimated from the brightness of the incandescent light of the sample to be roughly 1000°C. After cooling, the nature of the crystalline phases of the sample was studied by in situ x-ray diffraction (MoK_α radiation) while the sample remained at full pressure between the diamond anvil faces. After completion of the in situ study, pressure was released and the sample was transferred to a modified 57.3-mm Debye-Scherrer camera for x-ray analysis of the quenched sample with CuK_α radiation.

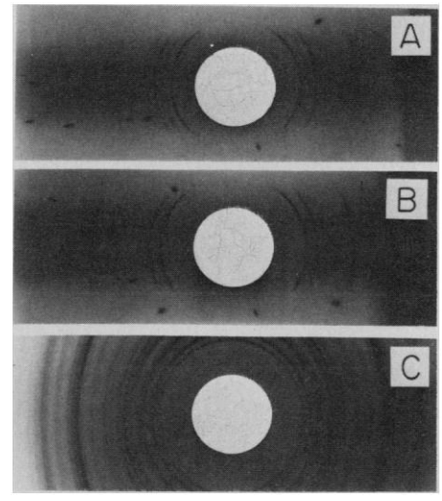

Fig. 1. (A) The x-ray diffraction pattern (MoK_α) of SnO_2 at about 250 kbar and room temperature (before being heated by laser). It is primarily the rutile phase (cassiterite) with four weak, unidentified lines which may correspond to the pressure-induced phase of SnO_2 reported in (*16*). (B) X-ray diffraction pattern (MoK_α) of the same sample after laser heating but before pressure release, at room temperature. The main phase (> 95 percent) is the cubic fluorite modification of SnO_2. Details of the x-ray diffraction data of this pattern are shown in Table 1. (C) The X-ray pattern (CuK_α) of the quenched SnO_2 shown in (B), after pressure release, at atmospheric pressure and room temperature. It consists of a two-phase mixture of cassiterite and the α-PbO_2 form of SnO_2.

Figure 1A shows the diffraction pattern of the SnO_2 sample at about 250 kbar and room temperature (before being heated by laser). The pattern consists of the rutile phase (cassiterite) plus four weak, unidentified lines. These unknown lines may correspond to the "apparent" high-pressure phase of SnO_2 at about 250 kbar and room temperature reported by Clendenen and Drickamer (*16*). The most intense line (interplanar spacing d = 2.839 Å) corresponds to the most intense line (111) of the cubic fluorite-type SnO_2 to be described in this report. Figure 1B shows the x-ray pattern of the same sample, after laser heating but before pressure release, at room temperature. The pattern can be indexed entirely as the cubic fluorite phase of SnO_2, except for three very weak lines. Two of these may correspond to the starting cassiterite, and third one is not known yet. Details of the x-ray data are shown in Table 1. Figure 1C shows the x-ray pattern of the quenched sample at atmo-

Table 1. Room temperature x-ray diffraction data for SnO_2 and TiO_2 at about 250 kbar (MoK_α). Samples were heated by a continuous yttrium-aluminum-garnet laser at about 250 kbar in a diamond-anvil pressure cell.

SnO_2				TiO_2			
Observed		Fluorite type		Observed		Hexagonal form	
I/I_{100}	d (Å)	d (Å)	hkl	I/I_{100}	d (Å)	d (Å)	hkl
15	3.22	Cassiterite	(110)	5	2.83	2.84	002
100	2.842	2.844	111			2.678	102
				100	2.667	2.667	211
70	2.466	2.463	200			2.663	300
10	2.211	2.203	201(?)	10	2.410	2.411	301
5	2.03	Cassiterite	(210)	20	2.302	2.306	220
60	1.743	1.741	220	30	1.664	1.667	411
60	1.483	1.485	311	5	1.609	1.605	213
15	1.423	1.422	222	5	1.510	1.510	420
5	1.226	1.231	400	10	1.420	1.421	004
20	1.130	1.130	331	5	1.379	1.375	403
20	1.101	1.101	420				
10	1.004	1.005	422				
a = 4.925 ± 0.005 Å				a = 9.22 ± 0.01 Å			
Z = 4				c = 5.685 ± 0.006 Å			
V = 17.99 cm³/mole				Z = 16			
8 percent volume change at transition				V = 15.75 cm³/mole			
				8.5 percent volume change at transition			

spheric pressure and room temperature (after release of pressure). This pattern is nearly identical to an earlier one of a quenched product of SnO_2 from 155 kbar (*8*). It consists of a two-phase mixture of cassiterite and the α-PbO_2 form of SnO_2.

Thus, the experimental results demonstrate that the cubic fluorite structure is the true postrutile phase of SnO_2, and that the α-PbO_2 form appears only on pressure release from fluorite-type SnO_2. It is possible that, as for PbO_2, the α-PbO_2 structure of SnO_2 has a very limited stability field between the rutile and the fluorite fields of SnO_2, so that on pressure release the fluorite-type SnO_2 reverts to the α-PbO_2 structure.

On the basis of the two weak lines of cassiterite (Fig. 1B and Table 1) and the available compression data of cassiterite (*16*), the pressure of the sample was estimated to be 240 kbar. The room-temperature lattice parameter of the fluorite-type SnO_2 at the applied pressure is calculated to be $a = 4.925 \pm 0.005$ Å and the volume, V, is 17.99 ± 0.05 cm^3/mole, about 8 percent smaller than that of cassiterite at the transition. The latter value is in good agreement with the zero-pressure volume change (~ 11 percent) associated with the transition from rutile to fluorite in SnO_2 that I have estimated (*17*).

An in situ x-ray diffraction study of TiO_2, after laser heating at about 150 kbar, has revealed four diffraction lines of the α-PbO_2 structure (110, 111, 121, and 112) in addition to the starting rutile. The stability field for the α-PbO_2 form of TiO_2 thus appears to be well established. An entirely different x-ray diffraction pattern was obtained for TiO_2 at a maintained loading pressure of about 250 kbar after laser heating. Details of the x-ray data are listed in Table 1. These diffraction lines were indexed as hexagonal with $a = 9.22 \pm 0.01$ Å and $c = 5.685 \pm 0.006$ Å. No known structure can be readily assigned to the new phase. However, on the basis of existing knowledge of the volume changes associated with the transitions from rutile to postrutile in difluorides and dioxides, a value of Z (number of formula units per cell) = 16 is tentatively assigned for the new phase. This value yields V of 15.75 ± 0.05 cm^3/mole at about 250 kbar, about 8.5 percent smaller than that of the α-PbO_2 form (or 10.5 percent smaller than that of rutile), at the transition. The latter figure is comparable with the zero-pressure volume change (~ 13 percent) that I have estimated for the transition from rutile to fluorite (*17*). I therefore believe that the new phase is related to the fluorite structure. The new phase is not quenchable; it reverts to the α-PbO_2 form on pressure release.

A plot of shock velocity versus particle velocity from all the available shock-wave experiments (*13, 14*) appears to warrant only one phase transformation each for SnO_2 and TiO_2. The zero-pressure volume change associated with the apparent shock-induced transition is greater by at least a factor of 2 than those observed for the transition from rutile to fluorite found in the present study. However, the results of the shock experiments (*13, 14*) do not rule out the possibility of the occurrence of a transition from rutile to fluorite in SnO_2 and TiO_2 if it were followed by a further transition. This is so because only the arrival of the first wave could be detected in the shock experiments of (*13, 14*). Instead, those experiments show that, if a transition from rutile to fluorite occurs, it must be followed by a further transition, possibly to the α-$PbCl_2$ structure (which is about 10 percent denser than the fluorite structure). The finding of the α-PbO_2 form of SiO_2 by recovery shock experiment (*5*) should not be taken as indicative of the occurrence of the fluorite or its related forms of SiO_2. This conclusion should not be drawn for several reasons. (i) German *et al.* had some doubts about the results of the shock experiment (*5*), which Liu *et al.* pointed out (*6*). (ii) The α-PbO_2 form of SiO_2 was not confirmed by static high-pressure experiments (*6*). (iii) The hypothetical transition from rutile to fluorite for SiO_2 involves some 18 percent change in the zero-pressure volume (*17*), whereas no detectable discontinuity in the density of the Hugoniot data of SiO_2 was found between 400 and 6500 kbar (*18*).

I have shown that the postspinel phase of Mg_2SiO_4 is the assemblage of $MgSiO_3$ (orthorhombic perovskite) plus MgO (periclase) (*19*) and that the ilmenite forms of $MgSiO_3$ and $(Mg_{0.75}Al_{0.25})(Al_{0.25}Si_{0.75})O_3$ transform directly to their stoichiometric perovskite phases at pressures relevant to the onset of the earth's lower mantle (*20*). Since the assemblages containing the orthorhombic perovskite phase are (at zero pressure and room temperature) 2 to 3 percent denser than their corresponding mixed oxide phases containing stishovite, I have concluded that the earth's lower mantle is primarily composed of mineral assemblages containing the perovskite phases of ferromagnesian silicate instead of oxide phases as in Birch's hypothesis (*21*). This conclusion is not altered when the effect of pressure on the compressibility of the various phases is taken into consideration. Only if SiO_2 could acquire the fluorite or its related modifications at pressures not in excess of those of the earth's interior, as has been shown for SnO_2 and TiO_2 in the present study, would the hypothesis of a lower mantle (or core) composed of oxide phases become feasible.

The hypothetical fluorite-type SiO_2 was estimated to be about 20 percent denser than stishovite at zero pressure (*17*). Taking a simplified earth mantle with 60 mole percent olivine plus 40 mole percent pyroxene as an example (*21*), the zero-pressure density for the mixture SiO_2 (fluorite) plus MgO (periclase) is 5.8 percent greater than that of the assemblage $MgSiO_3$ (perovskite) plus MgO (periclase). This difference in density may be acceptable for the earth's lower mantle within the present resolution of seismic observation. Thus the possibility that the lower mantle is composed of oxide phases might exist if the fluorite or its related structures of SiO_2 could be experimentally synthesized at high pressure and temperature conditions. However, a distinction should still be made between Birch's oxide hypothesis, which assumes that the primary coordination of silicon is 6, and that for possible oxide phases with coordination 8 in the lower mantle as suggested here.

LIN-GUN LIU*
Seismological Laboratory, California Institute of Technology, Pasadena 91125

References and Notes

1. F. Birch, *J. Geophys. Res.* **57**, 227 (1952).
2. S. M. Stishov and S. V. Popova, *Geokhimiya* **10**, 837 (1961).
3. E. C. T. Chao, J. J. Fahey, J. Littler, D. J. Milton, *J. Geophys. Res.* **67**, 419 (1962).
4. Y. Syono and S. Akimoto, *Mater. Res. Bull.* **3**, 153 (1968).
5. V. N. German, M. A. Podurets, R. F. Trunin, *Sov. Phys. JETP* **37**, 107 (1973); V. N. German, N. N. Orlova, L. A. Tarasova, R. F. Trunin, *Bull. Acad. Sci. USSR Earth Phys.* **11**, 431 (1975).
6. L. Liu, W. A. Bassett, J. Sharry, *J. Geophys. Res.*, in press.
7. P. Ruetschi and B. D. Cahan, *J. Electrochem. Soc.* **104**, 406 (1957).
8. L. Liu, *Phys. Earth Planet. Inter.* **9**, 338 (1974).
9. F. Dachille and R. Roy, *Am. Ceram. Soc. Bull.* **41**, 225 (1962); N. A. Bendeliani, S. V. Popova, L. F. Vereshchagin, *Geochem. Int.* **3**, 387 (1966).
10. L. M. Azzaria and F. Dachille, *J. Phys. Chem.* **65**, 889 (1961).
11. S. S. Kabalkina and S. V. Popova, *Sov. Phys. Dokl.* **8**, 1141 (1964).
12. L. F. Vereshchagin, S. S. Kabalkina, A. A. Kotilevits, *Sov. Phys. JETP* **22**, 1181 (1966); S. S. Kabalkina, L. F. Vereshchagin, L. M. Lityagins, *Sov. Phys. Dokl.* **12**, 946 (1968); D. P. Dandekar and J. C. Jamieson, *Trans. Am. Crystallogr. Assoc.* **5**, 19 (1969).
13. R. G. McQueen and S. P. Marsh, unpublished data; G. V. Simakov, M. A. Podurets, R. F. Trunin, *Dokl. Akad. Nauk SSSR* **211**, 29 (1973).
14. R. G. McQueen, J. C. Jamieson, S. P. Marsh, *Science* **155**, 1401 (1967); L. V. Altshuler, M. A. Podurets, G. V. Simakov, R. F. Trunin, *Sov. Phys. Solid State* **15**, 969 (1973).
15. W. A. Bassett, T. Takahashi, P. W. Stook, *Rev. Sci. Instrum.* **38**, 37 (1967).
16. R. L. Clendenen and H. G. Drickamer, *J. Chem. Phys.* **44**, 4223 (1966).
17. L. Liu, *Phys. Earth Planet. Inter.* **10**, 344 (1975).
18. R. F. Trunin, G. V. Simakov, M. A. Podurets,

B. N. Moiseyev, L. V. Popov, *Izv. Acad. Sci. USSR Phys. Solid Earth* **1**, 13 (1970).
19. L. Liu, *Nature (London)* **262**, 770 (1976).
20. ———, *Earth Planet. Sci. Lett.* **31**, 200 (1976); *Science* **195**, 990 (1977).
21. ———, *Geophys. J. R. Astron. Soc.* **48**, 53 (1977); *Earth Planet. Sci. Lett.* **36**, 237 (1977).
22. I thank J. R. Cleary for commenting on the manuscript. This research was supported by the California Institute of Technology's President Venture Fund. Contribution No. 2941, Division of Geological and Planetary Sciences, California Institute of Technology.
* On leave of absence from the Research School of Earth Sciences, Australian National University, Canberra, A.C.T., Australia.

18 July 1977; revised 12 September 1977

Far-Ultraviolet Stopped-Flow Circular Dichroism

Abstract. *A stopped-flow circular dichroism instrument, with a total accessible wavelength range of 200 to 750 nanometers, has been constructed and provides a spectroscopic method for kinetic investigations of a wide array of fast reactions in which optical activity changes in absorbing regions are involved. An important biochemical application depends on the far-ultraviolet capability, which allows observation of the rapid alterations in backbone conformation associated with folding and unfolding reactions of proteins. Results obtained by following two such reactions at 222 nanometers represent direct monitoring by circular dichroism of rapid secondary structure changes in proteins.*

The elucidation of the detailed processes involved in biological macromolecular folding represents a fundamentally important area of current biochemical research (*1*, *2*). As part of an effort in that direction, we have been investigating thermodynamic and kinetic aspects of the folding from partially disordered states of separated, human α- and β-globin chains free of heme (α^0 and β^0). Early experiments (*3*, *4*) revealed the need for instrumentation which would provide a direct and interpretable probe of rapid secondary structure changes. Toward that end, we have constructed a prototype stopped-flow circular dichroism (SFCD) instrument with a time response in the millisecond range in the far-ultraviolet (UV) absorption region of the protein polypeptide backbone.

In contrast to light transmission and fluorescence—the parameters most often monitored in stopped-flow (SF) work—circular dichroism (CD), which measures differential absorbance of left- and right-circularly polarized light (*5*), is intrinsically sensitive to molecular asymmetry. The SFCD technique in the visible and near-UV was introduced by Bayley and Anson (*6*) with measurements of the changes in ligand-induced CD at selected wavelengths for several protein systems. More recently, Nitta *et al.* (*7*) have reported the application of SFCD for following changes in ellipticity at 270 nm of aromatic amino acid residues.

The CD associated with spectral transitions near 220 nm of the polypeptide backbone provides a direct measure, for a protein in solution, of the type and the extent of secondary structure (*8*). By use of a stabilized Xe light source, a 50-khz piezooptical birefringence modulator, and phase-sensitive, heterodyning lock-in amplification techniques, in conjunction with an observation chamber of novel optical and flow design (*9*) and a carefully constructed vibration-damping mount, we have overcome the considerable light energy and stability problems involved in making rapid far-UV measurements with acceptable signal-to-noise (S/N) ratios. Modifications are being made to improve signal sensitivity and time response by an order of magnitude. Details of the instrumental designs may be found elsewhere (*10*).

As examples of the application of the prototype instrument to monitor far-UV CD changes, we present here two experiments of importance to our hemoglobin studies. In the first we monitored partial refolding when a solution of disordered α^0 was brought from *p*H 4.5 to *p*H 5.8. In the second we measured the rapid acid denaturation of methemoglobin by following loss of α-helix as seen in the fall of CD intensity at 222 nm. It should be noted that in both cases the parameter being followed provided a measure of the rate of change in α-helix content. To our knowledge, the results represent the first direct detection of rapid secondary structure changes and allow isolation of one level of conformational change in complex systems where many occur.

The band pass at 222 nm was ~2.5 nm. Instrumental dead time, the time elapsed between the initiation of mixing and the beginning of accumulation of useful kinetic data, was 12 msec. The data, representing the difference in transmission between the 50-khz alternating left- and right-circularly polarized components—a value approximately 10^{-4} times the magnitude of the average light transmission—as normalized with respect to the average, were digitally recorded and displayed. To avoid distorting effects, the lock-in amplifier output smoothing time constant, τ_F, was always set at less than 0.1 times the value of the observed reaction lifetime. The photographs of the displayed data (see Figs. 1 and 2) show the raw data points from consecutive SF runs with no adjustment of instrumental setting or averaging. Each SF run involved an expenditure of 0.15 ml of reactant.

The α^0 was prepared and purified at *p*H 5.7 (20 m*M* phosphate) by the method of Yip and co-workers (*3*, *4*). The isolated monomer fraction was denatured by adjusting the *p*H to 4.5 with 1*M* KH_2PO_4. The jump to *p*H 5.8, carried out at 4°C, was accomplished by mixing with 20 m*M* K_2HPO_4 (see Fig. 1 and Table 1). The rise in the CD value of the *p*H-jumped globin represents an increase in the percentage of amino acid residues in the helical conformation (percent helicity)

Table 1. Stopped-flow 222-nm circular dichroism experiments. The concentrations of the initial protein reactant solutions were determined by absorbance measurements, using extinction coefficients for methemoglobin of $\epsilon_{500} = 9.04 \times 10^3$ and $\epsilon_{406} = 162 \times 10^3$ per heme (*13*) and for α^0 of $\epsilon_{277.5} = 10 \times 10^3$ (*3*). Static CD values were determined on a Cary recording spectropolarimeter in the static mode, using a model 6001 CD accessory. The actual SF dead time was 12 msec, but the apparent dead time depends on τ_F.

Experimental parameter	Renaturation of α^0	Denaturation of methemoglobin
*p*H of protein reactant solution	4.5	6.5
Final protein concentration, mole/liter	2.2×10^{-5}	1.8×10^{-5} (in heme)
Total CD signal		
Degrees	0.023	0.088
Degree cm^2 dmole^{-1} (mean residue)	3.7×10^3	17.2×10^3
Associated noise level, millidegrees	~5	~17
Second reactant	20 m*M* K_2HPO_4	HCl
*p*H of second reactant	9.5	1.31, 1.76*, 2.26
Final *p*H of mixture	5.8	1.55, 2.05, 2.55
Total time span of photograph, seconds	102.4	1.02, 1.02, 5.1
$\tau_{1/2}$, milliseconds		
Approximate from photograph		48, 110, 455
From digital analysis	5000	42, 124, 415

*Photograph not shown.

0036-8075/78/0127-0425$00.50/0